Mikada, H., Moore, G.F., Taira, A., Becker, K., Moore, J.C., and Klaus, A. (Eds.)
Proceedings of the Ocean Drilling Program, Scientific Results Volume 190/196

3. Provenance of Miocene–Pleistocene Turbidite Sands and Sandstones, Nankai Trough, Ocean Drilling Program Leg 190[1]

Christopher L. Fergusson[2]

ABSTRACT

During Ocean Drilling Program Leg 190 several turbidite successions in the Nankai Trough were drilled through including Pleistocene trench fill (Sites 1173 and 1174), Pleistocene–Pliocene slope basin deposits and underlying trench fill (Sites 1175 and 1176), Miocene Shikoku Basin deposits (Site 1177), and upper Miocene trench fill (Site 1178). Sands from the Pleistocene trench-fill succession of the Nankai Trough are of mixed derivation with significant monomineralic components (quartz and feldspar) and mafic to intermediate volcanic rock fragments, in addition to sedimentary and less abundant metamorphic detritus. They have a source in the Izu collision zone in central Honshu. Sands from the slope and accreted trench fill at Sites 1175 and 1176 are dominated by quartz with less abundant feldspar, sedimentary rock fragments, and only minor volcanic and metamorphic rock fragments. In contrast to the trench turbidites of Sites 1173 and 1174, these sands are very quartzose with characteristic radiolarian chert fragments. Volcanic rock fragments are mainly of silicic composition. Potential sources of these sands are uplifted subduction complexes of southwest Japan. Sands from the accreted trench turbidites at Site 1178 have clast types similar to those at Sites 1175 and 1176. In contrast, however, framework detrital modes are distinctive, with Site 1178 sands having substantially lower total quartz contents and more abundant fine-grained sedimentary rock fragments. These sands were also probably derived from the island of Shikoku, but their composition indicates that sedimentary rocks

[1]Fergusson, C.L., 2003. Provenance of Miocene–Pleistocene turbidite sands and sandstones, Nankai Trough, Ocean Drilling Program Leg 190. *In* Mikada, H., Moore, G.F., Taira, A., Becker, K., Moore, J.C., and Klaus, A. (Eds.), *Proc. ODP, Sci. Results,* 190/196, 1–28 [Online]. Available from World Wide Web: <http://www-odp.tamu.edu/publications/190196SR/VOLUME/CHAPTERS/205.PDF>. [Cited YYYY-MM-DD]
[2]School of Geosciences, University of Wollongong, NSW 2522, Australia.
cferguss@uow.edu.au

Initial receipt: 6 November 2002
Acceptance: 5 August 2003
Web publication: 14 November 2003
Ms 190SR-205

were abundant in the source area and these may have been Miocene forearc basin successions that were largely removed by erosion. Erosional remnants of Miocene forearc basin deposits are present on the Kii Peninsula east-northeast of Shikoku. Erosion followed a phase of exhumation of the Shimanto Belt indicated by apatite fission track ages at ~10 Ma. Sand in the lower–upper Miocene turbidites of the lower Shikoku Basin section at Site 1177 is more varied in composition, with the upper part of the unit similar to Site 1178 (i.e., rich in sedimentary rock fragments) and the lower part similar to those at Sites 1175 and 1176 (i.e., rich in quartz with some silicic volcanic rock fragments). Sands from the lower part of the Miocene turbidite unit were derived from a continental source with plutonic and volcanic rocks, possibly the inner zone of southwest Japan.

INTRODUCTION

Ocean Drilling Program (ODP) Leg 190 was concerned with coring and sampling five sites (Sites 1173–1176 and 1178) along the Muroto Transect across the Nankai Trough accretionary prism (Fig. F1) (Moore, Taira, Klaus, et al., 2001; Moore et al., 2001). The Muroto Transect is southeast of Cape Muroto in southwest Japan and includes ODP Site 808 (Leg 131). An additional site was drilled to the west (Site 1177) that, along with some Deep Sea Drilling Project (DSDP) sites (Leg 87, Sites 582 and 583), provided a second transect (the Ashizuri Transect) (Fig. F1). The main objectives of Leg 190 were to (1) examine the structure of the Nankai Trough accretionary prism and find its relationship to diagenesis and fluids and (2) provide constraints on the contrasting stratigraphic and structural development of the accretionary prism along strike. Previous workers (De Rosa et al., 1986; Taira and Niitsuma, 1986; Marsaglia et al., 1992; Underwood et al., 1993) have shown that sands in the Nankai Trough were derived from several main sources since the Pliocene and are a reflection of the complex tectonics of the region including uplift of the Shimanto subduction complex on Shikoku and island arc collision in central Honshu.

This paper concerns sand composition and provenance from all Leg 190 sites and complements previous studies of Nankai Trough sands. The main aim is to document framework detrital modes of sand/sandstone sampled during Leg 190 deep-sea drilling for the first time including a Pliocene–Pleistocene lower trench-slope basin, late Miocene accreted trench fill of the Nankai Trough accretionary prism, and Miocene turbidite facies of the Shikoku Basin succession. Three sand petrofacies are recognized (volcaniclastic, quartzose, and sedimenticlastic), and these demonstrate the wide variations in sand compositions that can be encountered in a subduction zone setting. Tentative conclusions about the provenance of Leg 190 sands also provide some constraints on the sediment dispersal pattern in a subduction zone setting, namely, the role of transverse delivery of sands down the trench-slope as opposed to longitudinal sand supply along the trench (e.g., Dickinson, 1982).

F1. Site location map, p. 16.

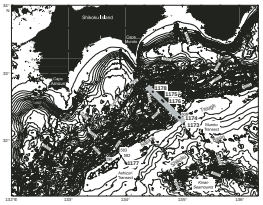

TECTONIC SETTING AND LEG 190 LITHOSTRATIGRAPHY

The tectonic history of Japan over the last 20 m.y. is complicated and involves the development of a major collision zone in central Honshu between the Honshu arc and the Izu-Bonin island arc (Taira et al., 1989). Japan was part of the Asian mainland prior to the major spreading in the Japan Sea at 15–18 Ma (Tamaki et al., 1992; Jolivet et al., 1994; Lee et al., 1999). Subduction was active throughout the Cretaceous and early Tertiary in southwest Japan with development of a subduction complex (Shimanto Belt) that includes rocks as young as early Miocene on Cape Muroto (Taira et al., 1988). The Nankai Trough accretionary prism continues to form by the subduction of the Philippine Sea plate as it converges under southwest Japan (Eurasian plate) in a northwest direction at a rate estimated at ~40 mm/yr (Seno et al., 1993). The Neogene history of subduction along the Nankai Trough is far from clear; for example, Niitsuma (1988) suggested that subduction has been active since at least 7 Ma, whereas Maruyama et al. (1997) portrayed subduction as continuous throughout the Neogene. Island arc collision between the Izu-Bonin and Honshu arcs began at ~12 Ma and was episodic with four major accretion events at ~12, 7–9, 3–5, and ~1 Ma (Amano, 1991; cf. Niitsuma, 1989). The last of these events is responsible for the influx of sediment along the Nankai Trough as seen in the upper Pleistocene sediments at Sites 1173, 1174, and 808. Uplift of the Tertiary and older subduction complexes in southwest Japan were inferred by fission track ages to occur at ~10 Ma in Shikoku and earlier at ~15 Ma on the Kii Peninsula (Hasebe et al., 1993; Tagami et al., 1995).

The subducting Philippine Sea plate underlies the Nankai Trough and consists of 15- to 26-m.y.-old igneous basaltic basement. Outboard of the Nankai Trough in the Shikoku Basin, eruptions continued up to ~12 Ma on the Kinan Seamounts (Fig. **F1**) (Kobayashi et al., 1995). Miocene–Pleistocene mud and turbidites of the Shikoku Basin succession overlies the basaltic basement.

At Site 1177, the lower Shikoku Basin succession consists of a lower Miocene silicic volcaniclastic unit overlain by a lower–upper Miocene siliciclastic turbidite unit (Shipboard Scientific Party, 2001b). Neither of these units is present in the Muroto Transect. At Site 297, located ~90 km south of Site 1177, Unit 4 consists of early Pliocene turbidites similar in composition to those at Site 1177 but apparently younger (Shipboard Scientific Party, 1975b, 2001b). At Site 808 (Leg 131) the Shikoku Basin succession has a basal volcaniclastic unit with abundant thick-bedded silicic sandy to muddy volcaniclastic layers derived from the ~14-Ma silicic volcanism and plutonic activity that affected the southeastern zones of southwest Japan (Shipboard Scientific Party, 1991). The upper Shikoku Basin succession at Site 1177 and in the Muroto Transect has a lower unit of silty clay(stone) and an upper unit of silty clay with interbedded ash layers (Moore, Taira, Klaus, et al., 2001). The boundary between these units is diagenetically controlled by the breakdown of ash layers in the lower unit.

The Nankai Trough is partly filled by a wedge of trench turbidites that thicken toward the deformation front at the base of the accretionary prism (Fig. **F2**). At Sites 808, 1174, and 1173 these turbidites are of late Pleistocene age (<1 Ma) (Moore, Taira, Klaus, et al., 2001), whereas farther west at Site 298, early Pleistocene thin-bedded turbidites were also recorded (Shipboard Scientific Party, 1975a). Mafic intermediate

F2. Summary stratigraphic columns, p. 17.

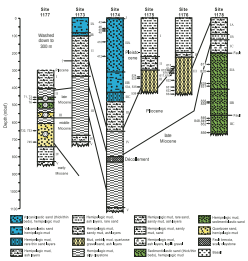

volcanic detritus, quartz, and feldspar with a minor component of sedimentary and metamorphic debris dominate these sands and were derived from the island arc collisional zone in central Honshu (Taira and Niitsuma, 1986; Underwood et al., 1993).

Three Leg 190 sites are located on the lower trench slope (Sites 1175, 1176, and 1178) in the northwestern part of the Muroto Transect (Fig. F2). Sites 1175 and 1176 penetrated a trench-slope basin and encountered an upper unit of hemipelagic mud and ash layers with many contorted and slumped horizons that reflect downslope gravitational movement of unconsolidated materials (Moore, Taira, Klaus, et al., 2001). Unit II at both sites consists of hemipelagic mud, sandy mud to muddy sand, ash layers, and rare silt to sand turbidites. At both sites the lowest unit is a slope to underlying accreted trench fill of late early Pliocene to early Pleistocene age. In contrast to the upper Pleistocene trench fill at Site 1174, fine-grained sedimentary fragments, including chert, dominate the trench fill sandstone, pebbly mudstone, and gravel at Sites 1175 and 1176. At Site 1178 an upper unit of slope mud, ash, and sand is underlain by accreted upper Miocene trench fill of the Nankai Trough accretionary prism (Moore, Taira, Klaus, et al., 2001). Given the relatively young ages and proximity to land it is clear that the Japanese Islands are the source of sand and gravel encountered in Leg 190 cores.

METHODS

Samples were wet sieved to remove clay and dried in an oven before impregnation and thin sectioning. Thin sections were etched with concentrated hydrofluoric acid and stained with sodium cobaltinitride (yellow stain after K-feldspar) and amaranth (pink stain after calcic plagioclase). Albite is etched but not affected by staining and is distinguished from quartz by twinning and alteration in untwinned crystals. Staining also aids identification of silicic volcanic rock fragments and was particularly significant in the deeper samples from Site 1177. Where possible, sands with medium to coarse grain sizes were selected for point counting (39 slides from a total of 95 slides), but the remaining samples with fine to very fine grain size were examined. Stratigraphic setting of modally analyzed samples is shown on Figure F2. The Gazzi-Dickinson method of point counting was followed, where sand-sized crystals included in lithic fragments are counted as the mineral component to overcome the effect of grain size (Ingersoll et al., 1984). This method has the advantage that the results from different grain sizes can be compared and is particularly relevant given the variation in grain sizes between the different sites. A total of 500 points of sand grains were counted for each thin section. The numbers of raw points for each category can be calculated by multiplying the percentages in Table T1 by five. Although counted, carbonate, organic material, and intraformational clay debris were not included in the 500-point total (raw counts are shown in Table T1). Volcanic rock fragments with both lathwork and microlitic textures (Dickinson, 1970) are present, but given the abundance of compositionally indeterminate mafic to intermediate fragments at Site 1174 this classification as used in some previous studies (Marsaglia et al., 1992) was not attempted.

T1. Modal analyses sands, Nankai Trough, p. 21.

SAND COMPOSITION

Sand and sandstone samples from Leg 190 are split into three major petrofacies related to different stratigraphic units in the Nankai Trough region (Fig. F2). These petrofacies consist of the following:

1. Volcaniclastic sands at Sites 1173 and 1174,
2. Quartzose sands at Sites 1175 and 1176, and
3. Sedimenticlastic sandstones at Site 1178.

Sands and sandstones from Site 1177 include both quartz-rich and sedimenticlastic types. Apart from Site 1177 there were minimal vertical variations in mineral and clast types in sand and sandstone at Leg 190 sites.

Sites 1173–1174: Volcaniclastic Sands

These samples are all from the upper Pleistocene axial trench-wedge facies of the Nankai Trough (Subunit IIA at Site 1174 and Unit I at Site 1173). Site 1173 sands are fine to very fine grained, but petrographic analysis shows that they are compositionally similar to those at Site 1174. Sands at both sites are poorly sorted and consist mainly of angular to subangular grains. Modes were only determined for Site 1174 samples (Table T1). Modally analyzed sands at Site 1174 are medium to very coarse. The sands are all lithic rich and plot near the L (lithic fragments) corner on a QFL (quartz-feldspar-lithic) diagram (Fig. F3A) and near the Lv (volcanic lithic fragments) corner on a LmLvLs (metamorphic lithic–volcanic lithic–sedimentary lithic) plot (Fig. F3B). Mafic to intermediate volcanic rock fragments are dominant with common sedimentary lithic fragments, plagioclase, and quartz (Plate P1).

Quartz

Quartz (7%–21%) is the most abundant mineral component and has both straight and undulose extinction. Fine-grained quartzite and vein quartz are relatively uncommon. Grains of chert, some with recrystallized radiolarians, are relatively rare.

Feldspar

Feldspar (17%–22%) is common and consists mainly of relatively fresh plagioclase. Plagioclase is present as a common phenocryst mineral in the volcanic rock fragments. Many plagioclase crystals contain small glassy blebs and mineral inclusions (Plate P1). K-feldspar is present in all samples (1%–4%).

Mineral Fragments

Additional mineral fragments are minor (<8%) and include pyroxene, olivine, hornblende, biotite, and opaque minerals. These minerals are present as phenocryst phases in volcanic rock fragments. Rare metamorphic and igneous minerals such as chlorite, epidote, and, less commonly, tourmaline are present.

F3. Sand and sandstone plots, p. 18.

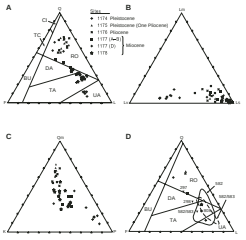

P1. Mineral and lithic grains from sands, Site 1174, p. 25.

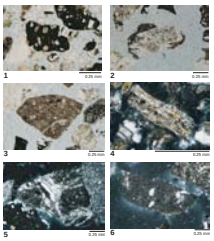

Volcanic Rock Fragments

Volcanic rock fragments are the most common component (25%–46%) and are dominated by mafic to intermediate varieties. These fragments typically consist of phenocrysts and microphenocrysts of olivine, pyroxene, plagioclase, and, more rarely, hornblende contained in an altered black and/or brown glassy groundmass (Plate P1). Many of the porphyritic volcanic grains may well be of basaltic andesitic affinity. Felsic volcanic fragments are more easily distinguished by the presence of quartz (1%–8%), although some of these grains are difficult to distinguish from chert and some sedimentary lithic fragments. The presence of phenocrysts and devitrification textures distinguishes some felsic fragments. Fresh colorless glass is relatively rare.

Sedimentary Lithic Fragments

Sedimentary lithic fragments are common (18%–32%). They are mainly mudstone fragments, some with thin quartz veins, and fine-grained siliceous rock fragments. Rare fine-grained quartzose sandstone, lithic sandstone, and quartz siltstone fragments are present.

Metamorphic Rock Fragments

Metamorphic rock fragments are minor (<8%) and are mainly metamorphosed sedimentary and volcanic rock fragments. The sedimentary rock fragments are typically low-grade slates and in Sample 190-1174B-1R-1, 6–10 cm, include some rare biotite-bearing hornfels. Metamorphosed volcanic rock fragments contain chlorite and epidote. Rare plutonic rock fragments distinguished by graphic intergrowths are present in Sample 190-1174A-3H-5, 69–73 cm. Most plutonic detritus is counted under monomineral component fragments, owing to the use of the Gazzi-Dickinson point-counting method.

Sites 1175 and 1176: Quartzose Sands

These samples come from the lower part of Units II and III (Pliocene–Pleistocene) at Sites 1175 and 1176 (Fig. F2). The modally analyzed samples are medium to very coarse, poorly sorted sands and pebbly sands with dominantly angular to subangular grains. They contain abundant quartz, sedimentary rock fragments, and minor feldspar. Site 1175 and 1176 samples overlap near the Q corner on the QFL plot (Fig. F3A). On the LmLvLs plot they all occur near the Ls corner (Fig. F3B). Volcanic detritus is relatively minor in contrast to the axial trench sands at Sites 808, 1173, and 1174.

Quartz

Quartz (55%–72%) includes monocrystalline quartz including some grains exhibiting undulose extinction, incipient polygonal grains, and rare deformation bands. Polycrystalline quartz is also common and with common fragments of veins with comb structure. Chert is common (3%–23%) with black and red chert containing recrystallized radiolarian tests that are circular in thin section (Plate P2).

P2. Mineral and lithic grains from sands, Sites 1175 and 1176, p. 26.

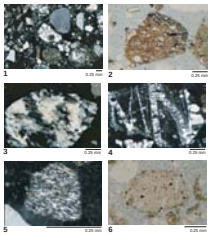

Feldspar

Feldspar is a persistent component (5%–24%) and consists mainly of plagioclase and altered fragments of probable untwinned albite. K-feldspar (3%–14%) includes rare grains of microcline with its distinctive cross-hatched twinning (Plate P2).

Mineral Fragments

Additional mineral fragments are relatively minor (<2%) and include low-grade metamorphic minerals such as muscovite, biotite, chlorite, and epidote. Others are rare and include pyroxene and hornblende, probably of igneous derivation, and rare tourmaline, garnet, and zircon.

Sedimentary Lithic Fragments

Sedimentary lithic fragments are common (10%–24%). They include fine-grained mudstone that is clearly lithified as shown by the presence of thin quartz veins (Plate P2) and easily distinguished from unconsolidated mud that was inadvertently included during the sampling process. Many fine-grained siliceous fragments are also present that are transitional to chert and polycrystalline quartz but contain more abundant impurities than fragments identified as chert. Rare fine-grained quartzose sandstone, lithic sandstone, and quartz siltstone fragments are present. Much of the vein quartz in these samples is most likely derived from sedimentary rocks including chert (e.g., Plate P2).

Volcanic Rock Fragments

Volcanic rock fragments are minor (<8%) and are dominated by felsic volcanic fragments. The presence of phenocrysts, flow textures, and spherulites distinguishes some felsic fragments (Plate P2). Rare mafic to intermediate volcanic fragments are present in some samples. Fresh and altered glass also is present but relatively rare (e.g., Sample 190-1175A-43X-3, 75–78 cm). Tube pumice only occurs in Sample 190-1175A-39X-CC, 10–13 cm.

Metamorphic Rock Fragments

Metamorphic rock fragments are also relatively minor (<5%) and are mainly metamorphosed sedimentary rock fragments. These consist of two main types: foliated quartz-chlorite fragments (impure quartzite) and unfoliated low-grade metamorphic rock fragments containing minerals such as epidote and chlorite. The presence of relict volcanic textures and the abundance of chlorite and epidote distinguish metamorphosed volcanic rock fragments. Some metamorphic rock fragments are too altered to distinguish their parent material. Fragments of slate are scarce.

Plutonic Rock Fragments

Plutonic rock fragments are distinguished by intergrowths of quartz and feldspar (e.g., graphic intergrowth) that is too fine to be recorded as separate mineral components. Most plutonic detritus is counted as crystal fragments.

Site 1177: Quartzose and Sedimenticlastic Sands and Sandstones

Sand and sandstone samples at Site 1177 are from Unit III, the lower–upper Miocene lower Shikoku Basin turbidite facies (Fig. F2). Many of the samples consist of very fine to fine sand and sandstone, but only fine to medium sand samples were modally analyzed. These sands are poorly sorted with angular to subangular grains and less common subrounded grains. Their finer grain sizes means that they are less suited for modal analysis than sands from Sites 1175 and 1176. Mineral and clast types in Site 1177 sands are similar to those from Sites 1175, 1176, and 1178 (Plate P3). Sand in the unit occurs in four sandy intervals, with interval D at the base and intervals C, B, and A in ascending order to the top of the unit (Shipboard Scientific Party, 2001b). The four sand samples modally analyzed from sand interval A and the top of sand interval B contain subequal amounts of quartz (36%–47%), feldspar (20%–30%), and lithic fragments (22%–43%). Lithic fragments are dominantly of sedimentary type with a smaller quantity of silicic volcanic rock fragments (2%–5%). On the QFL diagram the sands from intervals A and B plot closer to sands from Site 1178 than those from Sites 1175 and 1176, whereas on the LmLvLs diagram they overlap with sands from Sites 1175 and 1176 (Fig. F3). The three samples analyzed from sand interval D have higher quartz content (54%–67%), similar feldspar content (21%–34%), and lower lithic content (11%–15%) than the samples from intervals A and B. The content of silicic volcanic fragments in interval D (2%–7%) is comparable to the upper intervals. On the QFL diagram the lower sands compositionally overlap those from Sites 1175 and 1176, whereas on the LmLvLs plot two samples plot with the sands from Site 1174 and one plots with sands from Sites 1175 and 1176 (Fig. F3).

P3. Mineral and lithic grains from sands/sandstones, Site 1177, p. 27.

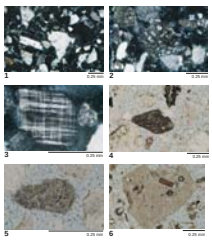

Site 1178: Sedimenticlastic Sandstones

The Site 1178 samples are all from Unit II, which consists of upper Miocene accreted trench-wedge facies (Fig. F2). The sandstones are medium to very coarse and poorly sorted with subrounded to angular grains. The larger grains are usually more rounded than the smaller grains. Compared to samples from most other sites they are dominated by sedimentary lithic fragments (mudstone, siltstone, fine sandstone, and siliceous claystone) (Plate P4) with minimal chert. On the QFL plot they lie near Site 1174 sands, but they have only lower quartz content in common with these sediments (Fig. F3A). On the LmLvLs plot they plot on or very close to the Ls corner (Fig. F3B). Clast types are similar to those for Sites 1175, 1176, and 1177 but the overall proportions differ with lower total quartz and higher lithic fragments compared with these other sites:

- **Quartz** (23%–36%) includes monocrystalline quartz, polycrystalline quartz, and chert (<5%).
- **Feldspar** is common with subequal plagioclase and K-feldspar (9%–21%).
- **Additional mineral fragments** are rare (<1%) and include muscovite, chlorite, epidote, garnet, and zircon.
- **Sedimentary lithic fragments** are abundant (49%–59%) and are mainly mudstone and less common quartz sandstone, lithic sandstone, and quartz siltstone fragments.

P4. Mineral and lithic grains from sands/sandstones, Site 1178, p. 28.

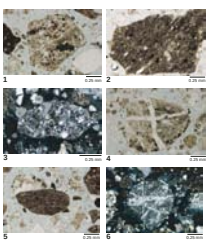

Volcanic rock fragments are minor (<6%) and are mainly felsic volcanic fragments.

Metamorphic rock fragments are minor (<5%) and are mainly low-grade metamorphosed sedimentary rock fragments.

Provenance

Petrographic discrimination diagrams, such as those created by Dickinson and Suczek (1979) and Dickinson et al. (1983), are useful indicators of distinctive source regions with implications for the tectonic setting of the Japan region (e.g., Marsaglia et al., 1992) and Leg 190 sand provenance. Late Pleistocene sands from Sites 1173 and 1174 have similar compositions to other Nankai Trough trench wedge Sites 808, 582, and 583 (Fig. F1); these plot in the undissected to transitional arc field on a QFL diagram (Fig. F3A, F3D) (De Rosa et al., 1986; Taira and Niitsuma, 1986; Marsaglia et al., 1992; Underwood et al., 1993). Five of the samples analyzed from Site 1174 fall in the undissected arc field (Fig. F3A). Miocene and Pliocene–early Pleistocene sands from Sites 1175, 1176, and 1177 (sand interval D) plot in the recycled orogen field (Fig. F3A). Site 1178 late Miocene sandstones plot on the QFL diagram in the transitional arc and dissected arc fields, and Site 1177 (sand intervals A and B) sandstones plot on the recycled orogen dissected arc boundary (Fig. F3A). On the LmLvLs diagram Site 1174 sands are easily distinguished from all other sites apart from two samples (Site 1177, sand interval D) that contain small quantities of lithic fragments (Fig. F3B). The distinction is clearer on the QmKP diagram where Site 1174 sands plot close to the plagioclase corner in a separate group from the other Leg 190 sites (Fig. F3C).

DISCUSSION

The lower Shikoku turbidite facies (Unit III at Site 1177) is of early–late Miocene age (~6–16 Ma) and therefore represents a major period of deposition in the Shikoku Basin although at a relatively low sedimentation rate of ~30 m/m.y. (Shipboard Scientific Party, 2001b). Sandstones at Site 1177, sand interval D, are latest early–middle Miocene age and are older than all other medium to coarse sand encountered during Leg 190 (Fig. F2) (Shipboard Scientific Party, 2001b). These sands are dominated by quartz and feldspar with lower lithic fragments that in two samples are mainly felsic volcanic fragments and in the other are mainly sedimentary rock fragments (Table T1). The greater quartz and feldspar content of these sands is consistent with derivation from a plutonic terrane; the source is difficult to identify on the basis of sandstone petrography alone. Further constraints from sediment geochemistry, isotopic data (e.g., U/Pb zircon ages), and zircon/apatite fission tracks are required to identify an appropriate source. A source is tentatively suggested as the inner zone of southwest Japan (Fig. F4). At this time emergent southwest Japan was dominated by Cretaceous and younger plutonic and volcanic rocks of the inner zone. This would imply a transverse delivery of sediment from the northwest into the Shikoku Basin (Fig. F4).

Initiation of deposition of the lower Shikoku Basin turbidite succession (Unit III at Site 1177) coincides with several major events in the Japanese region including rapid opening of the Japan Sea at 18–15 Ma (Otofuji, 1996; Lee et al., 1999). Also a phase of major igneous activity

F4. Major accretionary units of the outer zone of southwest Japan, p. 19.

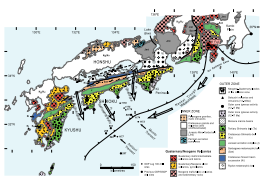

affected the outer zone of southwest Japan at 13–15 Ma with dominantly felsic plutonic rocks and associated volcanics (Fig. F4) (Hasebe et al., 1993) and with less volumetrically significant high-Mg andesite magmatism of the Setouchi volcanic belt (Figs. F4, F5) at ~13–14 Ma (Tatsumi et al., 2001). The Miocene outer zone igneous activity produced the rhyolitic tuffs discovered near the base of Site 808 (Shipboard Scientific Party, 1991), but no equivalents are present at Site 1177. The low content of volcanic material in the turbidites of sand interval D contrasts with the tuffaceous units at Site 808 and the underlying Unit IV at Site 1177.

Subduction may have been at least episodically active during the Miocene along the proto-Nankai Trough as indicated by (1) collision between the Honshu arc and the Izu-Bonin island arc in four main phases over the last 12 m.y. (Amano, 1991), (2) crustal shortening along the north coast of southwest Japan in the late Miocene (5–8 Ma) (Itoh and Nagasaki, 1996), and (3) resumption of widespread calc-alkaline volcanic activity in Kyushu at ~6 Ma (Kamata and Kodama, 1994). The continuing influx of sandy sediment into the Shikoku Basin at Site 1177 indicates that if subduction was occurring throughout deposition of the turbidite succession (6–16 Ma), then the trench and/or trough did not prevent sediment transport. If subduction occurred at the present rate of 40 mm/yr, then the turbidites at Site 1177 were derived from settling from turbidity currents that traveled as far as 600 km beyond the deformation front at the base of the proto-Nankai Trough accretionary prism. Deposition of the upper part of the turbidite succession at Site 1177 was synchronous with deposition of the axial and outer trench wedge facies at Site 1178 (Shipboard Scientific Party, 2001c). Thus, the Nankai Trough must have existed as a paleogeographic feature in the late Miocene (cf. Shipboard Scientific Party, 1975b) and this indicates that subduction was active from at least 7.5 Ma.

Late Miocene sandstone and sand from the upper part of Site 1177 (sand intervals A and B) and Site 1178 are similar to each other but contrast with those from Sites 1175 and 1176 in their significantly lower quartz content (Table T1; Figs. F3, F5). The lower quartz content is displaced by greater abundance of sedimentary rock fragments (Fig. F3; Table T1). Their quartz content is consistent with derivation from a continental land mass. This is also indicated by the abundance of woody plant material, especially in the upper parts of turbidite layers (Shipboard Scientific Party, 2001b). The commonly lower chert content of these sands compared with those from Sites 1175 and 1176 indicate that the Shimanto Belt was an unlikely source of these sediments (see below). Significant sedimentary rocks must have been present in the source area in addition to the uplifted subduction complexes and metamorphic rocks present throughout southwest Japan (Fig. F4) (Taira et al., 1988; Isozaki, 1996).

The timing of the provenance change between the lower–middle Miocene sandstone of interval D at Site 1177 to the upper Miocene sands/sandstones at Site 1177 is poorly constrained because of the limited data from sands in intervals C and much of B at Site 1177. On Shikoku Island, cooling of the Shimanto Belt at ~10 Ma is indicated by apatite fission track data and is interpreted to result from exhumation of the accretionary prism triggered by growth related to the Outer Zone felsic igneous activity supplying sediment to the trench (Tagami et al., 1995, p. 227). Sand derived from Outer Zone magmatism was not detected in samples from Site 1177.

F5. Sedimentation compared to Neogene and Quaternary events, p. 20.

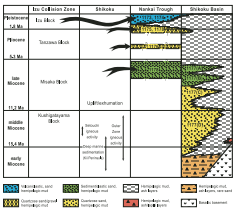

Upper Miocene sands from both the Nankai Trough and the turbidite succession of the Shikoku Basin contain only minor felsic volcanic detritus, which indicates that they are unlikely to derive from either the Kii Peninsula or Kyushu, where 13- to 15-Ma felsic igneous rocks are more abundant (Fig. F4). It is tentatively suggested, based solely on the sedimenticlastic sand composition and the lower chert content compared to Site 1175 and 1176 sands, that these upper Miocene units reflect erosion of lower–middle Miocene forearc basin deposits on Shikoku. Only small remnants of these units are preserved in the Shimanto Belt on Shikoku (Taira et al., 1988), but they are more widespread on the Kii Peninsula (Hisatomi, 1988). It is inferred that these deposits were formerly more widespread on Shikoku but were largely removed by erosion. Determination of sediment geochemistry and isotopic signatures of Leg 190 sediments and comparison with forearc basin sedimentary successions on Shikoku Island and the Kii Peninsula is required to substantiate this inference.

Pleistocene–Pliocene sands at Sites 1175 and 1176 are dominantly quartzose and lack mafic to intermediate volcanic rock fragments thought to characterize sand derived from the collision zone in central Honshu (Taira and Niitsuma, 1986; Marsaglia et al., 1992; Underwood et al., 1993). The abundance of sedimentary rock fragments and chert is consistent with derivation from the nearby uplifted subduction complexes of the Shimanto Belt in Shikoku (Fig. F4) (see fig. 22 in Taira and Niitsuma, 1986). The sands were presumably transported from the north-northwest down the inner trench slope rather than by axial transport along the Nankai Trough. Submarine canyons developed along the inner trench slope of the Nankai Trough extend up onto the continental shelf (Okino and Kato, 1995). These features or ones of similar geometry probably existed on the inner trench slope in the Pliocene–early Pleistocene when these sands were deposited. This confirms shipboard observations and the inference that a local southwest Japan source provided the trench fill to slope transition at Sites 1175 and 1176 (Moore, Taira, Klaus, et al., 2001).

The upper Pleistocene volcaniclastic sands at Sites 1173 and 1174 contain abundant mafic to intermediate volcanic fragments with less common sedimentary and metamorphic fragments and are consistent with derivation from the east in the collision zone between the Izu-Bonin and Honshu island arcs (Figs. F4, F5) (Taira and Niitsuma, 1986). Marsaglia et al. (1992) noted that sands from east to west along the Nankai Trough plotted on a mixing line between an undissected magmatic arc component and an accretionary prism component on a QFL triangular diagram. Sand from Sites 582 and 583 lay in the transitional arc field, whereas sand from Site 298 lay in the dissected arc field and sand from Site 297 lay on the boundary between the dissected arc field and the recycled orogen field (Fig. F3D). The implication is that along the trough to the west the uplifted subduction complex (recycled orogen) provided sediment to the trough and that this increased with distance from the Izu collisional zone. Site 1175 and 1176 sands represent the Shikoku end-member on the mixing line for Pleistocene sands in the Nankai Trough (Marsaglia et al., 1992).

CONCLUSIONS

In summary, Leg 190 sands and sandstones consist of three main petrofacies:

1. Volcaniclastic sand rich in mafic to intermediate rock fragments present in the upper Pleistocene section at Sites 1173 and 1174 and derived from the Izu collision zone at the eastern end of the Nankai Trough,
2. Quartzose sandstone with abundant quartz, less common feldspar, and lithic fragments present in the lower–middle Miocene section at Site 1177 and the Pliocene–lower Pleistocene sections at Sites 1175 and 1176, and
3. Sedimenticlastic sand and sandstone with abundant sedimentary lithic fragments present in the upper Miocene section at Sites 1177 and 1178.

A transverse delivery of sediment from northwestern sources (southwest Japan) is implied for the Miocene–lower Pleistocene quartzose and sedimenticlastic sand and sandstone at Leg 190 Sites 1175–1178, whereas the upper Pleistocene sands at Sites 1173 and 1174 are derived by lateral transport from the east along the Nankai Trough. These conclusions are limited because of the reliance on sandstone petrography and can be tested by analysis of the geochemistry of minerals, mud/mudstone and sand/sandstone samples, and radiometric dating of selected minerals from Leg 190 sections and comparison with inferred sources in southwest and central Japan.

ACKNOWLEDGMENTS

This research used samples provided by the Ocean Drilling Program (ODP). ODP is sponsored by the U.S. National Science Foundation (NSF) and participating countries under management of Joint Oceanographic Institutions (JOI), Inc. Funding for this research was provided by a grant from the Australian Office for the Ocean Drilling Program. The author is grateful for the reviews of Dr. Kathleen Marsaglia and Dr. Wonn Soh and editorial input from Dr. Asahiko Taira and Lorri Peters. Dr. Kathleen Marsaglia made many helpful suggestions, particularly in regard to sandstone nomenclature. The author remains entirely responsible for any deficiencies in the manuscript. At the University of Wollongong, Dave Carrie skillfully made many thin sections and provided other technical assistance. Thin sections were stained at Macquarie University (arranged by Dr. Norm Pearson). Peter Johnson drafted the figures.

REFERENCES

Amano, K., 1991. Multiple collision tectonics of the South Fossa Magna in central Japan. *Mod. Geol.,* 15:315–329.

de Rosa, R., Zuffa, G.G., Taira, A., and Leggett, J.K., 1986. Petrography of trench sands from the Nankai Trough, southwest Japan: implications for long-distance turbidite transportation. *Geol. Mag.,* 123:477–486.

Dickinson, W.R., 1970. Interpreting detrital modes of graywacke and arkose. *J. Sediment. Petrol.,* 40:695–707.

————, 1982. Compositions of sandstones in circum-Pacific subduction complexes and fore-arc basins. *AAPG Bull.,* 66:121–137.

Dickinson, W.R., Beard, L.S., Brakenridge, G.R., Erjavec, J.L., Ferguson, R.C., Inman, K.F., Knepp, R.A., Lindberg, F.A., and Ryberg, P.T., 1983. Provenance of North American Phanerozoic sandstones in relation to tectonic setting. *Geol. Soc. Am. Bull.,* 94:222–235.

Dickinson, W.R., and Suczek, C.A., 1979. Plate tectonics and sandstone compositions. *AAPG Bull.,* 63:2164–2182.

Geological Survey of Japan, 1982. Geological map of Japan, Scale 1:1,000,000 (3rd ed.). *Geol. Surv. Jpn.*

Hasebe, N., Tagami, T., and Nishimura, S., 1993. The evidence of along-arc differential uplift of the Shimanto accretionary complex: fission track thermochronology of the Kumano acidic rocks, southwest Japan. *Tectonophysics,* 224:327–335.

Hisatomi, K., 1988. The Miocene forearc basin of southwest Japan and the Kumano Group of the Kii Peninsula. *Mod. Geol.,* 12:389–408.

Ingersoll, R.V., Bullard, T.F., Ford, R.L., Grimm, J.P., Pickle, J.D., and Sares, S.W., 1984. The effect of grain size on detrital modes: a test of the Gazzi-Dickinson point-counting method. *J. Sediment. Petrol.,* 54:103–116.

Isozaki, Y., 1996. Anatomy and genesis of a subduction-related orogen: a new view of geotectonic subdivision and evolution of the Japanese Islands. *Isl. Arc,* 5:289–320.

Itoh,Y., and Nagasaki, Y., 1996. Crustal shortening of southwest Japan in the late Miocene. *Isl. Arc,* 5:337–353.

Jolivet, L.K., Tamaki, K., and Frounier, M., 1994. Japan Sea, opening history and mechanism: a synthesis. *J. Geophys. Res.,* 99:22237–22259.

Kamata, H., and Kodama, K., 1994. Tectonics of an arc-arc junction: an example from Kyushu Island at the junction of the southwest Japan arc and the Ryukyu arc. *Tectonophysics,* 233:69–81.

Kobayashi, K., Kasuga, S., and Okino, K., 1995. Shikoku Basin and its margins. *In* Taylor, B. (Ed.), *Backarc Basins: Tectonics and Magmatism:* New York (Plenum), 381–405.

Lee, Y.S., Ishikawa, N., and Kim, W.K., 1999. Paleomagnetism of Tertiary rocks on the Korean Peninsula: tectonic implications for the opening of the East Sea (Sea of Japan). *Tectonophysics,* 304: 131–149.

Marsaglia, K.M., Ingersoll, R.V., and Packer, B.M., 1992. Tectonic evolution of the Japanese Islands as reflected in modal compositions of Cenozoic forearc and backarc sand and sandstone. *Tectonics,* 11:1028–1044.

Maruyama, S., Isozaki, Y., Kimura, G., and Terabayashi, M., 1997. Paleogeographic maps of the Japanese Islands: plate tectonic synthesis from 750 Ma to the present. *Isl. Arc,* 6:121–142.

Moore, G.F., Taira, A., Bangs, N.L., Kuramoto, S., Shipley, T.H., Alex, C.M., Gulick, S.S., Hills, D.J., Ike, T., Ito, S., Leslie, S.C., McCutcheon, A.J., Mochizuki, K., Morita, S., Nakamura, Y., Park, J.-O., Taylor, B.L., Yagi, H., and Zhao, Z., 2001a. Data report: Structural setting of the Leg 190 Muroto Transect. *In* Moore, G.F., Taira, A., Klaus, A., et al., *Proc. ODP, Init. Repts.,* 190 [CD-ROM]. Available from: Ocean Drilling Program, Texas A&M University, College Station TX 77845-9547, USA.

Moore, G.F., Taira, A., Klaus, A., et al., 2001. *Proc. ODP, Init. Repts.,* 190 [CD-ROM]. Available from: Ocean Drilling Program, Texas A&M University, College Station TX 77845-9547, USA.

Moore, G.F., Taira, A., Klaus, A., and Leg 190 Scientific Party, 2001. New insights into deformation and fluid flow processes in the Nankai Trough accretionary prism: Results of Ocean Drilling Program Leg 190. *Geochem. Geophys. Geosyst.,* 2:10.1029/2001GC000166.

Niitsuma, N., 1988. Neogene tectonic evolution of southwest Japan. *Mod. Geol.,* 12:497–532.

————, 1989. Collision tectonics in the southern Fossa Magna, central Japan. *Mod. Geol.,* 14:3–18.

Okino, K., and Kato, Y., 1995. Geomorphological study on a clastic accretionary prism: the Nankai Trough. *Isl. Arc,* 4:182–198.

Otofuji, Y., 1996. Large tectonic movement of the Japan Arc in late Cenozoic times inferred from paleomagnetism: review and synthesis. *Isl. Arc,* 5:229–249.

Seno, T., Stein, S., and Gripp, A.E., 1993. A model for the motion of the Philippine Sea Plate consistent with NUVEL-1 and geological data. *J. Geophys. Res.,* 98:17941–17948.

Shipboard Scientific Party, 1975a. Site 296. *In* Karig, D.E., Ingle, J.C., Jr., et al., *Init. Repts. DSDP,* 31: Washington, DC (U.S. Govt. Printing Office), 191–206.

————, 1975b. Site 297. *In* Karig, D.E., Ingle, J.C., Jr., et al., *Init. Repts. DSDP,* 31: Washington (U.S. Govt. Printing Office), 275–316.

————, 1991. Site 808. *In* Taira, A., Hill, I., Firth, J.V., et al., *Proc. ODP, Init. Repts.,* 131: College Station, TX (Ocean Drilling Program), 71–269.

————, 2001a. Leg 190 Summary. *In* Moore, G.F., Taira, A., Klaus, A., et al., *Proc. ODP, Init. Repts.,* 190, 1–87 [CD-ROM]. Available from: Ocean Drilling Program, Texas A&M University, College Station TX 77845-9547, USA.

————, 2001b. Site 1177. *In* Moore, G.F., Taira, A., Klaus, A., et al., *Proc. ODP, Init. Repts.,* 190, 1–91 [CD-ROM]. Available from: Ocean Drilling Program, Texas A&M University, College Station TX 77845-9547, USA.

————, 2001c. Site 1178. *In* Moore, G.F., Taira, A., Klaus, A., et al., *Proc. ODP, Init. Repts.,* 190, 1–108 [CD-ROM]. Available from: Ocean Drilling Program, Texas A&M University, College Station TX 77845-9547, USA.

Tagami, T., Hasebe, N., and Shimada, C., 1995. Episodic exhumation of accretionary complexes: fission-track thermochronologic evidence from the Shimanto Belt and its vicinities, southwest Japan. *Isl. Arc,* 4:209–230.

Taira, A., Katto, J., Tashiro, M., Okamura, M., and Kodama, K., 1988. The Shimanto Belt in Shikoku, Japan: evolution of Cretaceous to Miocene accretionary prism. *Mod. Geol.,* 12:5–46.

Taira, A., and Niitsuma, N., 1986. Turbidite sedimentation in the Nankai Trough as interpreted from magnetic fabric, grain size, and detrital modal analyses. *In* Kagami, H., Karig, D.E., Coulbourn, W.T., et al., *Init. Repts. DSDP,* 87: Washington (U.S. Govt. Printing Office), 611–632.

Taira, A., Tokuyama, H., and Soh, W., 1989. Accretion tectonics and evolution of Japan. *In* Ben-Avraham, Z. (Ed.), *The Evolution of Pacific Ocean Margins:* Oxford (Oxford Univ. Press), 100–123.

Tamaki, K., Suyehiro, K., Allan, J., Ingle, J.C., Jr., and Pisciotto, K.A., 1992. Tectonic synthesis and implications of Japan Sea ODP drilling. *In* Tamaki, K., Suyehiro, K., Allan, J., McWilliams, M., et al., *Proc. ODP, Sci. Results,* 127/128 (Pt. 2): College Station, TX (Ocean Drilling Program), 1333–1348.

Tatsumi, Y., Ishikawa, N., Anno, K., Ishizaka, K., and Itaya, T., 2001. Tectonic setting of high-Mg andesite magmatism in the SW Japan arc: K-Ar chronology of the Setouchi volcanic belt. *Geophys. J. Int.,* 144:625–631.

Underwood, M.B., Orr, R., Pickering, K., and Taira, A., 1993. Provenance and dispersal patterns of sediments in the turbidite wedge of Nankai Trough. *In* Hill, I.A., Taira,

A., Firth, J.V., et al., *Proc. ODP, Sci. Results,* 131: College Station, TX (Ocean Drilling Program), 15–34.

Figure F1. Leg 190 (solid circles) and previous ODP/DSDP drill sites (solid squares and cross) in the Nankai Trough. Shaded area is the location of the three-dimensional seismic survey (Moore, Taira, Klaus, et al., 2001). Figure adapted from figure F6 of the Leg 190 Summary in the Leg 190 *Initial Reports* volume (Shipboard Scientific Party, 2001a).

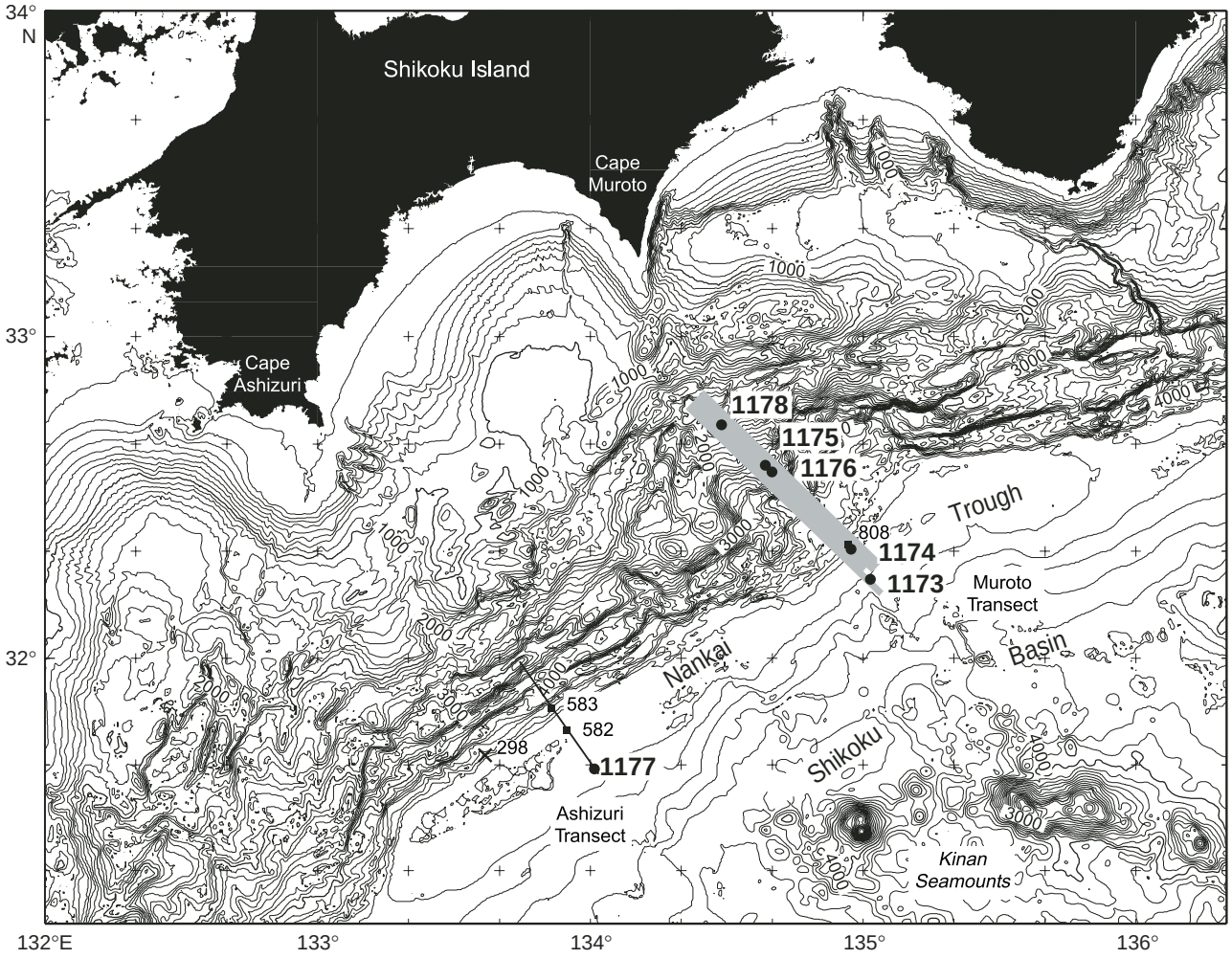

Figure F2. Summary stratigraphic columns of Leg 190 sites (after Moore, Taira, Klaus, et al., 2001). Sample locations of modally analyzed sands are shown on the left-hand side of each column. In the Site 1177 column the circled letters refer to the sandy intervals (see text).

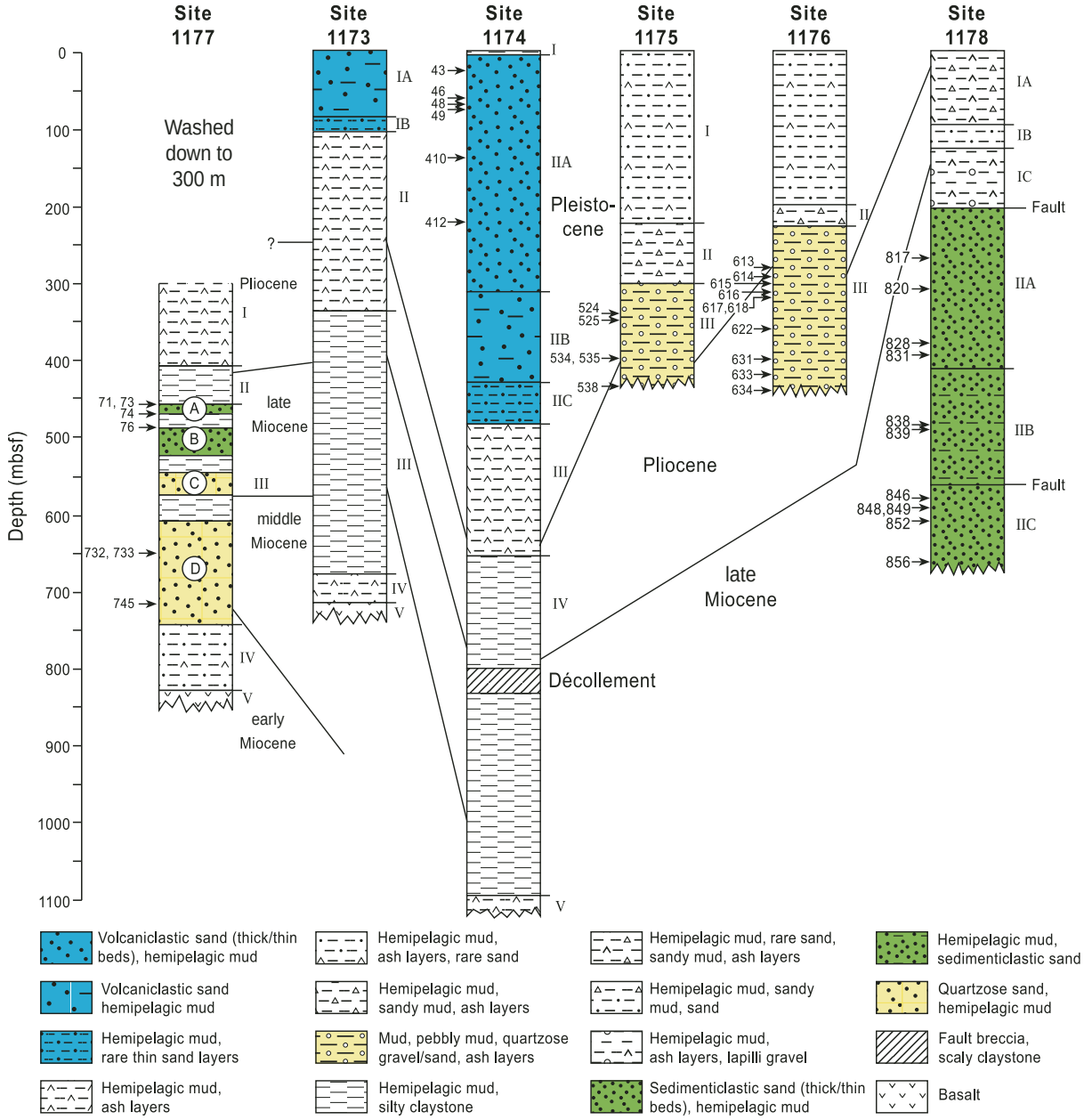

Figure F3. Sand and sandstone from Nankai Trough. (**A**) QFL (quartz-feldspar-lithic fragments), (**B**) LmLvLs (metamorphic-volcanic-sedimentary lithic fragments), and (**C**) QmKP (monocrystalline quartz–potassium feldspar–plagioclase feldspar) plots and (**D**) QFL plot with Leg 190 averages compared with averages of Sites 297, 298, 582/583 (Marsaglia et al., 1992), 808 (Shipboard Scientific Party, 1991), and fields of modes from Sites 582 (Taira and Niitsuma, 1986) and 582/583 (De Rosa et al., 1986). CI = craton interior, TC = transitional continental, BU = basement uplift, RO = recycled orogen, DA = dissected arc, TA = transitional arc, UA = undissected arc, QR = quartzose recycled, M = mixed, TR = transitional recycled, LR = lithic recycled. Provenance fields: Dickinson and Suczek (1979), Dickinson et al. (1983).

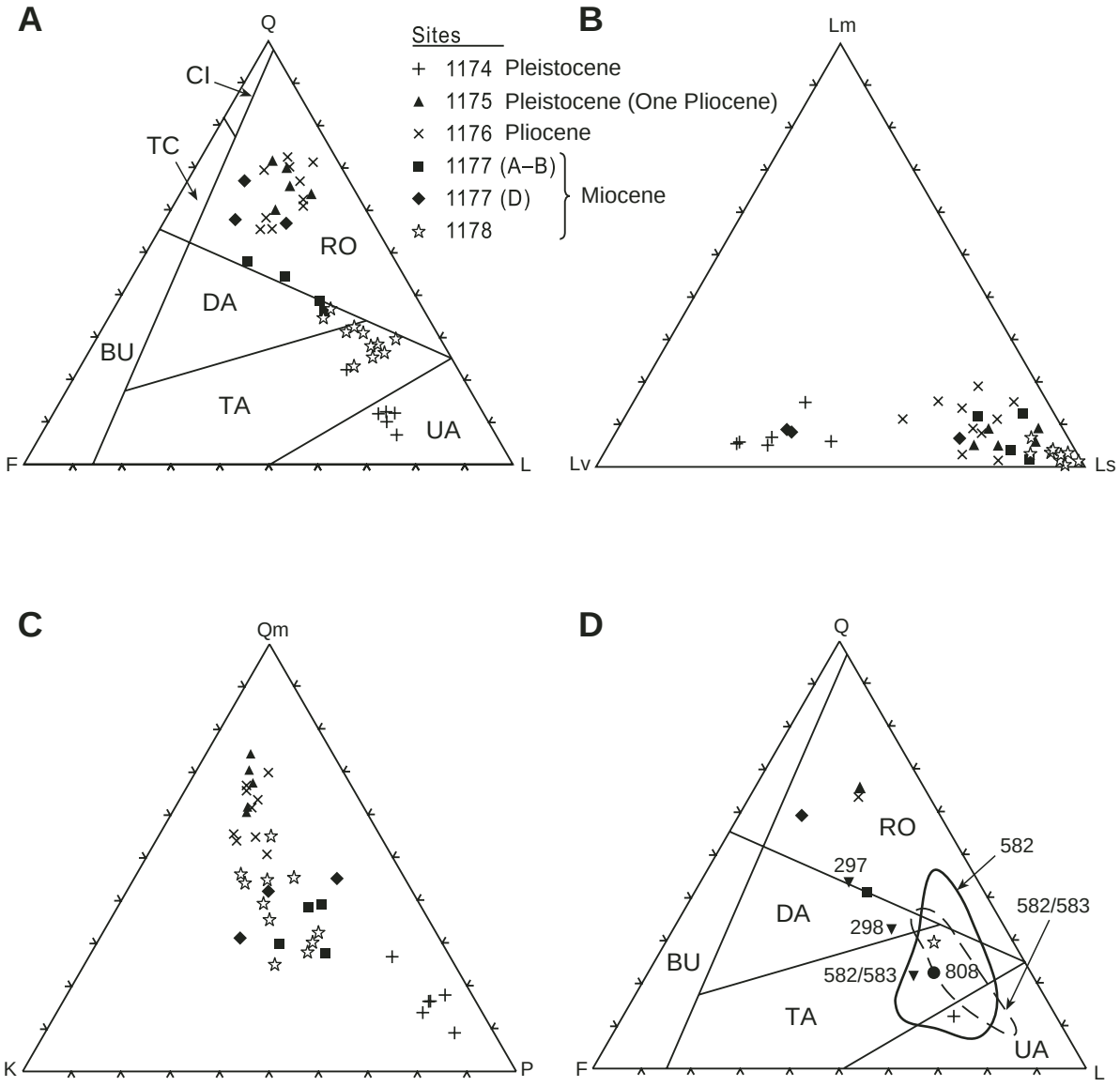

Figure F4. Simplified geological map of southwest and central Japan with the major accretionary units of the outer zone of southwest Japan depicted. The extent of Cretaceous granites and volcanics in Honshu and Kyushu includes older and younger units of lesser extent. Locations of Leg 190 and older drill sites are also shown. Inferred directions of sediment transport for the volcaniclastic (late Pleistocene), quartzose (Miocene and Pliocene–early Pleistocene), and sedimenticlastic (late Miocene) sand petrofacies are shown. Figure is compiled from the Geological Map of Japan (Geological Survey of Japan, 1992) and from figure F2 in the Leg 190 Summary of the Leg 190 *Initial Reports* volume (Shipboard Scientific Party, 2001a).

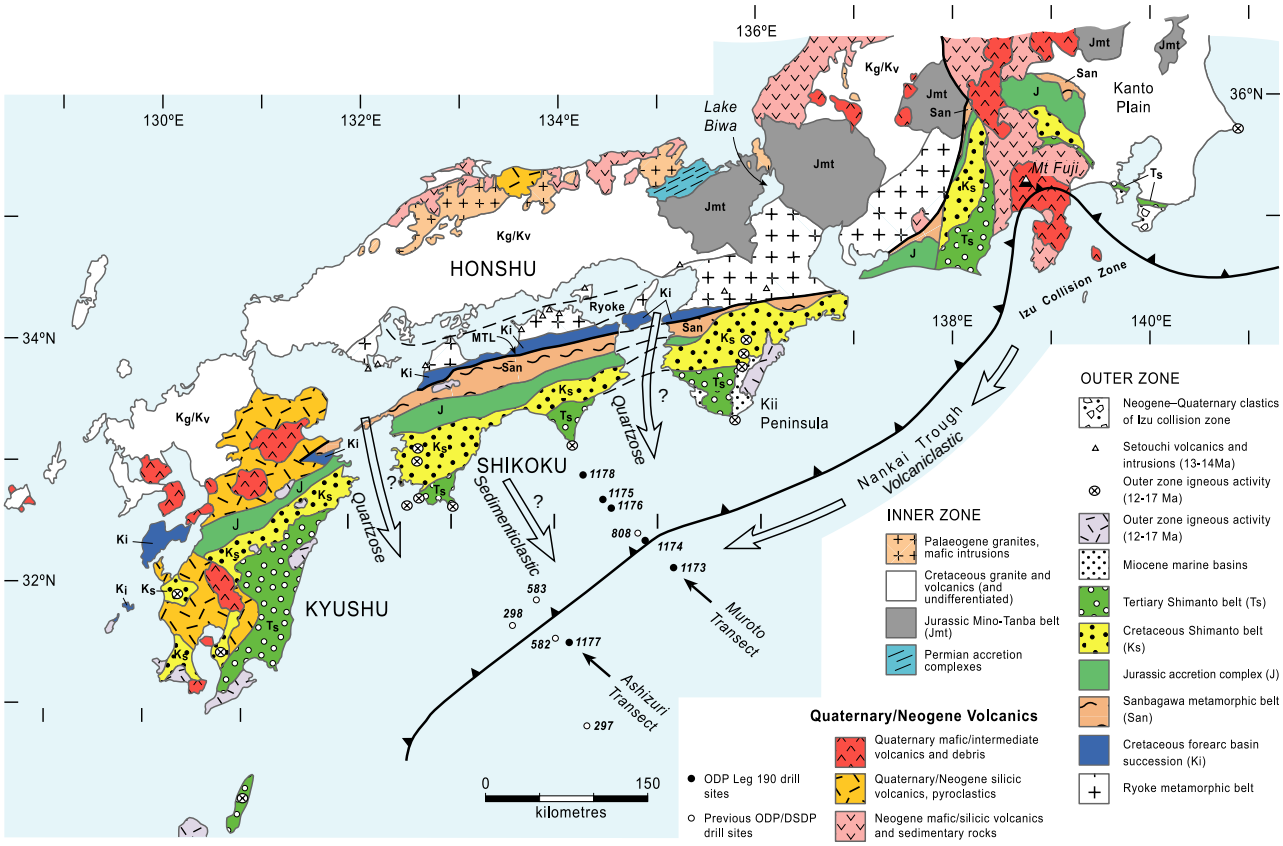

Figure F5. Time-space diagram with sedimentation in the Nankai Trough and Shikoku Basin compared to major Neogene and Quaternary events on Shikoku (Tagami et al., 1995; Tatsumi et al., 2001) and the four major episodes of accretion in the Izu collision zone (Amano, 1991).

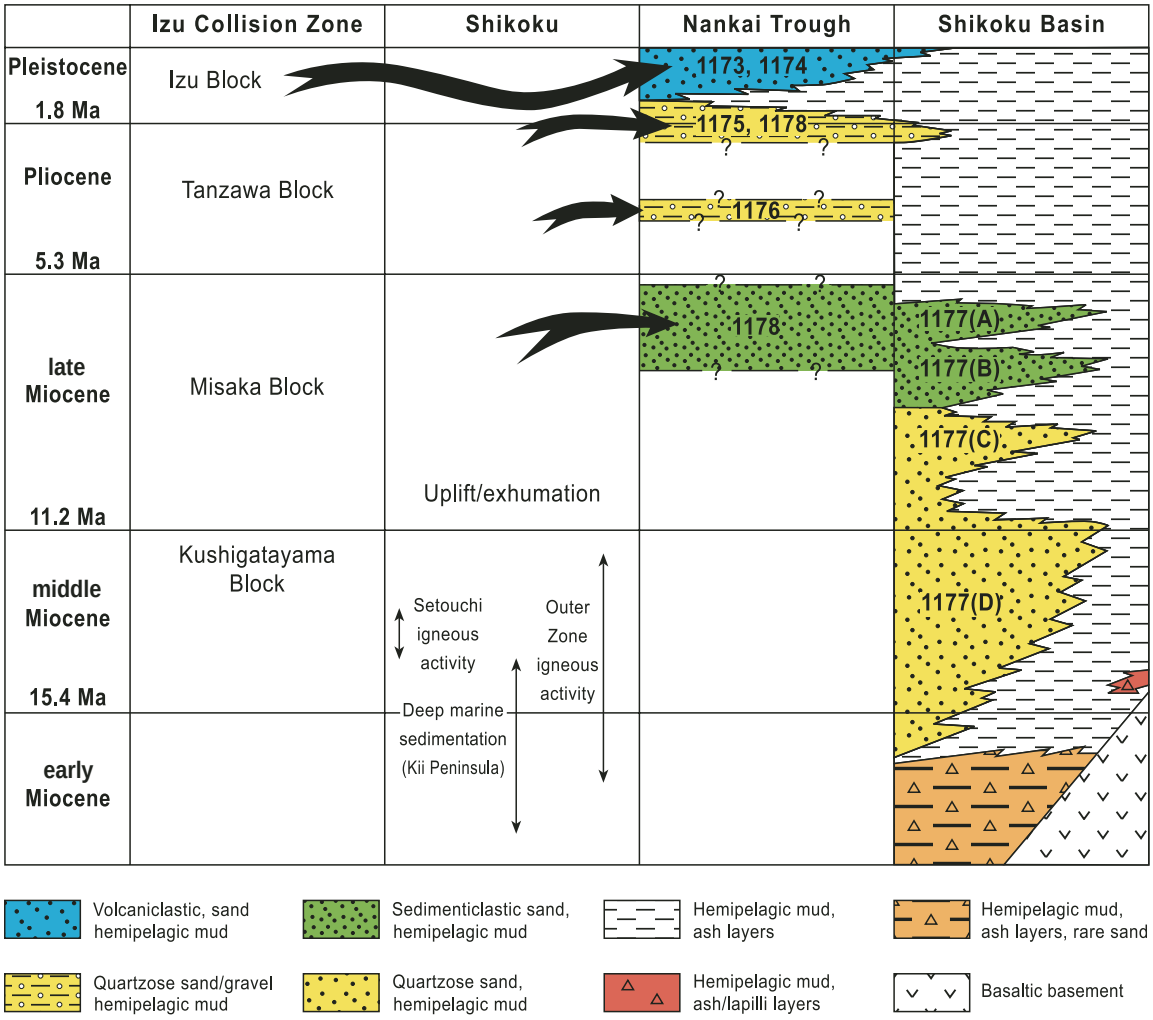

Table T1. Modal analyses of Leg 190 sands, Nankai Trough. (Continued on next three pages.)

Sample number:	43	46	48	49	410	412	524	525	534	535	538
Hole, core, section:	1174A-3H-5	1174A-8H-5	1174A-8H-CC	1174A-8H-CC	1174B-1R-1	1174B-9R-2	1175A-37X-1	1175A37X-4	1175A-43X-3	1175A-43X-3	1175A47X-CC
Interval (cm):	69–73	55–60	0–3	10–15	6–10	108–112	88–90	30–32	75–78	123–126	3–7
Qm (monocrystalline quartz)	8.2	3.8	3.8	4.0	2.0	3.2	21.6	27.2	28.6	26.6	26.8
Qmu (Qm with undulose extinction)	8.6	5.4	6.6	4.4	1.4	5.0	24.0	18.2	17.0	24.8	21.6
Qp (polycrystalline quartz)	4.0	2.0	0.8	2.0	1.4	1.2	13.0	15.0	8.0	9.2	11.2
Qp with a planar fabric							0.2			0.6	
Chert	0.4	0.2	0.4	0.4	1.8		12.4	8.8	5.0	3.6	3.0
P (plagioclase)	18.6	16.2	17.0	17.8	18.2	17.2	5.2	4.2	7.2	5.2	3.4
K (potassium)-feldspar	3.6	1.2	2.2	2.2	1.8	2.8	8.2	7.2	11.4	7.6	6.0
Ls (sedimentary rock fragments)	18.4	17.6	17.6	20.2	32.0	21.8	10.8	15.2	16.4	19.0	23.6
Lvf (felsitic volcanic rock fragments)	6.0	7.4	7.8	3.0	1.2	2.4	2.4	2.8	3.0	1.2	1.0
Lvm (mafic-intermediate Lv)	19.4	38.2	35.6	34.8	33.4	37.0	0.4			0.2	0.2
Lvg (volcanic glass)			0.6	0.4		0.8			0.2		
Lvtp (tube pumice)											
Lv (total volcanic rock fragments)	25.4	45.6	44.0	38.2	34.6	40.2	2.8	2.8	3.2	1.4	1.2
Lms (metasedimentary rock fragments)	4.8	3.0	2.4	1.4	2.4	1.0	0.4	1.0	2.0	1.0	2.6
Lmv (metavolcanic rock fragments)	1.8		1.0	1.8	1.4	2.2				0.2	
Lmu (unidentified Lm)	1.2	0.8	0.6		0.6	1.6	0.4			0.2	
Lp (plutonic clasts)	1.6	0.4	0.4		0.2		1.0	0.2		0.2	
Biotite	0.2			0.2		0.4		0.2			
Chlorite										0.2	
Epidote	1.4	0.4	0.2		0.2	0.2			0.6		0.2
Garnet									0.2		0.2
Hornblende	0.2			0.2							
Muscovite											0.2
Opaque minerals				0.2	0.2	0.2					
Pyroxene + olivine	1.6	3.4	3.0	7.0	1.8	2.6			0.4	0.2	
Tourmaline						0.4					
Zircon											
Total	100.0	100.0	100.0	100.0	100.0	100.0	100.0	100.0	100.0	100.0	100.0
Carbonate*	1	2	1	1	1		3	8			
Organic material*						1	1	1	1		5
Q (quartz) (%)	21.9	11.9	12.0	11.7	6.7	9.8	71.2	69.3	59.3	65.1	63.0
F (feldspar) (%)	23.0	18.1	19.8	21.6	20.4	20.8	13.4	11.4	18.8	12.9	9.5
L (lithic fragments) (%)	55.1	70.1	68.2	66.7	72.8	69.4	15.4	19.2	21.9	22.1	27.6
Lm (metamorphic lithic fragments) (%)	15.1	5.7	6.1	5.2	6.2	7.2	5.6	5.3	9.3	6.4	9.5
Lv (volcanic lithic fragments) (%)	49.2	68.1	67.1	62.0	48.7	60.2	19.4	14.7	14.8	6.4	4.4
Ls (sedimentary lithic fragments) (%)	35.7	26.3	26.8	32.8	45.1	32.6	75.0	80.0	75.9	87.2	86.1
(Chert + Qp)/Q	0.21	0.19	0.10	0.22	0.48	0.13	0.36	0.34	0.22	0.20	0.23
P/F	0.84	0.93	0.89	0.89	0.91	0.86	0.39	0.37	0.39	0.41	0.36
Lv/L	0.48	0.68	0.67	0.62	0.49	0.60	0.18	0.15	0.15	0.06	0.04
Qm (%)	27.0	17.9	16.5	16.7	9.1	13.8	61.7	70.5	60.6	67.5	74.0
K (%)	11.8	5.7	9.6	9.2	8.2	12.1	23.4	18.7	24.2	19.3	16.6
P (%)	61.2	76.4	73.9	74.2	82.7	74.1	14.9	10.9	15.3	13.2	9.4

Note: * = raw counts (not in 500 counts).

Table T1 (continued).

Sample number:	613	614	615	616	617	618	622	631	633	634	71
Hole, core, section:	1176A32X-CC	1176A-33X-CC	1176A34X-CC	1176A-35X-1	1176A-36X-2	1176A-40X-1	1176A-40X-1	1176A-44X-CC	1176A-46X-CC	1176A-48X-CC	1177A-16R-5
Interval (cm):	7–9	39–41	5–8	35–39	35–38	43–46	43–46	34–38	19–23	14–17	8–10
Qm (monocrystalline quartz)	23.8	26.0	26.6	21.2	13.6	23.4	24.4	32.4	8.8	16.8	15.2
Qmu (Qm with undulose extinction)	21.6	18.6	18.0	22.8	25.0	18.0	20.2	21.4	22.2	24.6	19.8
Qp (polycrystalline quartz)	8.8	7.2	9.4	13.0	11.4	10.6	6.0	8.8	15.4	20.0	6.4
Qp with a planar fabric	0.4								1.0	0.6	
Chert	5.2	2.8	3.8	12.6	11.8	14.4	4.0	6.2	23.2	10.0	2.6
P (plagioclase)	4.6	9.4	7.2	4.0	4.2	5.0	11.6	5.8	2.2	4.2	15.2
K (potassium)-feldspar	7.8	12.0	14.0	6.6	7.4	5.0	12.0	10.2	3.2	5.4	9.0
Ls (sedimentary rock fragments)	20.2	15.8	13.0	14.4	19.4	13.2	16.2	9.8	19.2	13.2	27.6
Lvf (felsitic volcanic rock fragments)	2.8	2.8	3.8	3.4	5.8	5.8	1.4	2.4	3.2	2.4	2.8
Lvm (mafic-intermediate Lv)	0.4		0.8	0.2	0.4	1.4		0.2	0.6	0.6	0.4
Lvg (volcanic glass)											
Lvtp (tube pumice)									0.2		
Lv (total volcanic rock fragments)	3.2	2.8	4.6	3.6	6.2	7.2	1.4	2.6	4.0	3.0	3.2
Lms (metasedimentary rock fragments)	2.4	3.2	2.0	1.8	0.8	2.4	3.2	1.8	0.4	1.2	0.6
Lmv (metavolcanic rock fragments)	0.6	0.4									
Lmu (unidentified Lm)		0.8	1.2			0.2		0.2		0.2	
Lp (plutonic clasts)	0.6					0.6		0.2	0.4	0.8	
Biotite											
Chlorite											
Epidote	0.4	0.8					0.4	0.6			
Garnet		0.2					0.4				
Hornblende	0.2										
Muscovite	0.2										0.2
Opaque minerals											
Pyroxene + olivine											
Tourmaline					0.2		0.2				0.2
Zircon			0.2								
Total	100.0	100.0	100.0	100.0	100.0	100.0	100.0	100.0	100.0	100.0	100.0
Carbonate*			12	3	12	3	3	1	17	4	
Organic material*		3	21	3	5	4	17	5	7	6	2
Q (quartz) (%)	60.3	55.2	57.9	69.6	61.9	66.4	55.2	69.2	70.6	72.0	44.2
F (feldspar) (%)	12.5	21.6	21.2	10.6	11.6	10.0	23.8	16.1	5.4	9.6	24.3
L (lithic fragments) (%)	27.2	23.2	20.8	19.8	26.5	23.6	21.0	14.7	24.0	18.4	44.2
Lm (metamorphic lithic fragments) (%)	11.4	19.1	15.4	9.1	3.0	11.3	15.4	13.9	1.7	8.0	1.9
Lv (volcanic lithic fragments) (%)	12.1	12.2	22.1	18.2	23.5	31.3	6.7	18.1	16.9	17.0	10.2
Ls (sedimentary lithic fragments) (%)	76.5	68.7	62.5	72.7	73.5	57.4	77.9	68.1	81.4	75.0	87.9
(Chert + Qp)/Q	0.23	0.18	0.23	0.37	0.38	0.38	0.18	0.22	0.55	0.42	0.20
P/F	0.37	0.44	0.34	0.38	0.36	0.50	0.49	0.36	0.41	0.44	0.63
Lv/L	0.12	0.12	0.22	0.18	0.23	0.31	0.07	0.18	0.17	0.16	0.10
Qm (%)	65.7	54.9	55.6	66.7	54.0	70.1	50.8	66.9	62.0	63.6	38.6
K (%)	21.5	25.3	29.3	20.8	29.4	15.0	25.0	21.1	22.5	20.5	22.8
P (%)	12.7	19.8	15.1	12.6	16.7	15.0	24.2	12.0	15.5	15.9	38.6

Table T1 (continued).

Sample number:	73	74	76	732	733	745	817	820	828	831	838
Hole, core, section:	1177A-17R-1	1177A-18R-1	1177A-20R-2	1177A-37R-3	1177A-37R-4	1177A-45R-1	1178A-30X-5	1178A-34X-1	1178A-42X-1	1178A-43X-3	1178B-11R-4
Interval (cm):	52–56	19–24	78–82	148–150	9–12	84–88	76–81	128–132	125–139	34–40	36–39
Qm (monocrystalline quartz)	8.8	13.0	11.6	20.4	17.8	15.8	12.4	14.6	13.2	11.6	11.0
Qmu (Qm with undulose extinction)	21.0	18.4	27.4	31.2	39.0	28.8	12.6	10.4	8.8	8.4	10.8
Qp (polycrystalline quartz)	4.2	5.4	6.6	3.6	7.0	5.2	3.8	3.4	3.0	4.6	3.2
Qp with a planar fabric								0.2	0.2		
Chert	2.0	1.6	1.6	2.0	2.8	4.2	2.2	2.6	2.4	4.6	1.0
P (plagioclase)	10.8	13.6	19.8	13.8	16.0	14.2	7.4	7.6	6.0	4.8	7.8
K (potassium)-feldspar	9.6	6.6	10.4	14.0	5.4	20.2	7.6	10.8	9.2	4.6	5.4
Ls (sedimentary rock fragments)	35.6	33.2	15.6	5.2	8.4	4.0	51.2	47.8	54.6	57.6	59.4
Lvf (felsitic volcanic rock fragments)	5.4	2.2	3.4	7.4	2.2	6.0	0.6	0.4	2.0	1.6	0.2
Lvm (mafic-intermediate Lv)		0.2		0.2	0.2	0.2	0.2	0.4		0.2	
Lvg (volcanic glass)	0.2	0.2	0.2	0.4	0.2	0.2					
Lvtp (tube pumice)											
Lv (total volcanic rock fragments)	5.6	2.6	3.6	8.0	2.6	6.4	0.8	0.8	2.0	1.8	0.2
Lms (metasedimentary rock fragments)	1.6	5.0	2.6	1.2	0.8	1.0	1.0	1.0	0.4	1.4	0.2
Lmv (metavolcanic rock fragments)							0.4				
Lmu (unidentified Lm)	0.2	0.2					0.6	0.8	0.2	0.6	0.8
Lp (plutonic clasts)	0.4	0.2		0.2	0.2						
Biotite											
Chlorite											
Epidote			0.8	0.2							0.2
Garnet						0.2					
Hornblende											
Muscovite	0.2										
Opaque minerals											
Pyroxene + olivine											
Tourmaline		0.2		0.2							
Zircon											
Total	100.0	100.0	100.0	100.0	100.0	100.0	100.0	100.0	100.0	100.0	100.0
Carbonate*	2	1	1	1			2	2	2	1	1
Organic material*	9		2		4	3		2	4	1	4
Q (quartz) (%)	36.1	38.5	47.6	57.4	66.6	54.1	31.0	31.2	27.6	29.2	26.1
F (feldspar) (%)	20.4	20.2	30.4	27.9	21.4	34.5	15.0	18.4	15.2	9.4	13.2
L (lithic fragments) (%)	43.5	41.3	22.0	14.7	12.0	11.4	54.0	50.4	57.2	61.4	60.7
Lm (metamorphic lithic fragments) (%)	4.2	12.7	11.9	8.3	6.8	8.8	3.7	3.6	1.0	3.3	1.7
Lv (volcanic lithic fragments) (%)	13.0	6.3	16.5	55.6	22.0	56.1	1.5	1.6	3.5	2.9	0.3
Ls (sedimentary lithic fragments) (%)	82.8	81.0	71.6	36.1	71.2	35.1	94.8	94.8	95.5	93.8	98.0
(Chert + Qp)/Q	0.17	0.18	0.17	0.10	0.15	0.17	0.19	0.19	0.20	0.32	0.16
P/F	0.53	0.67	0.66	0.50	0.75	0.41	0.49	0.41	0.39	0.51	0.59
Lv/L	0.13	0.06	0.17	0.55	0.22	0.56	0.01	0.02	0.03	0.03	0.00
Qm (%)	30.1	39.2	27.8	42.3	45.4	31.5	45.3	44.2	46.5	55.2	45.5
K (%)	32.9	19.9	24.9	29.0	13.8	40.2	27.7	32.7	32.4	21.9	22.3
P (%)	37.0	41.0	47.4	28.6	40.8	28.3	27.0	23.0	21.1	22.9	32.2

Table T1 (continued).

Sample number:	839	846	848	849	852	856
Hole, core, section:	1178B-12R-2	1178B-21R-2	1178B-23R-2	1178B-23R-2	1178B-25R-2	1178B-30R-3
Interval (cm):	32–33	66–71	45–47	133–135	51–53	15–20
Qm (monocrystalline quartz)	11.8	12.6	7.0	6.6	7.0	6.4
Qmu (Qm with undulose extinction)	13.6	11.6	9.8	13.0	12.2	18.2
Qp (polycrystalline quartz)	5.2	8.2	3.4	4.6	4.4	4.0
Qp with a planar fabric						
Chert	3.8	4.0	2.6	3.8	1.4	3.6
P (plagioclase)	10.6	9.2	10.8	8.8	10.0	9.8
K (potassium)-feldspar	10.6	10.0	10.2	4.8	6.0	6.4
Ls (sedimentary rock fragments)	41.4	40.6	47.2	53.2	51.6	48.4
Lvf (felsitic volcanic rock fragments)	1.4	2.0	4.0	2.6	4.8	1.6
Lvm (mafic-intermediate Lv)	0.2			0.2	0.6	
Lvg (volcanic glass)						
Lvtp (tube pumice)						
Lv (total volcanic rock fragments)	1.6	2.0	4.0	2.8	5.4	1.6
Lms (metasedimentary rock fragments)	0.8	1.6	3.6	2.0	1.4	1.6
Lmv (metavolcanic rock fragments)		0.2			0.2	
Lmu (unidentified Lm)	0.2		0.4	0.2	0.4	
Lp (plutonic clasts)			0.8	0.2		
Biotite						
Chlorite	0.4					
Epidote						
Garnet						
Hornblende						
Muscovite			0.2			
Opaque minerals						
Pyroxene + olivine						
Tourmaline						
Zircon						
Total	100.0	100.0	100.0	100.0	100.0	100.0
Carbonate*		2	1	2	1	1
Organic material*	3	7	6	2	4	2
Q (quartz) (%)	34.5	36.4	22.8	28.0	25.0	32.2
F (feldspar) (%)	21.3	19.2	21.0	13.6	16.0	16.2
L (lithic fragments) (%)	44.2	44.4	56.1	58.4	59.0	51.6
Lm (metamorphic lithic fragments) (%)	2.3	4.1	7.2	3.8	3.4	3.1
Lv (volcanic lithic fragments) (%)	3.6	4.5	7.2	4.8	9.2	3.1
Ls (sedimentary lithic fragments) (%)	94.1	91.4	85.5	91.4	87.5	93.8
(Chert + Qp)/Q	0.26	0.34	0.26	0.30	0.23	0.24
P/F	0.50	0.48	0.51	0.65	0.63	0.60
Lv/L	0.04	0.05	0.07	0.05	0.09	0.03
Qm (%)	35.8	39.6	25.0	32.7	30.4	28.3
K (%)	32.1	31.4	36.4	23.8	26.1	28.3
P (%)	32.1	28.9	38.6	43.6	43.5	43.4

Plate P1. Photomicrographs illustrating mineral and lithic grains from sands at Site 1174, Leg 190, Nankai Trough trench wedge. **1.** Mafic to intermediate volcanic rock fragments with microphenocrysts of plagioclase and pyroxene in a brown-black glassy groundmass (Sample 190-1174B-9R-2, 108–112 cm [220.3 mbsf]) (plane-polarized light). **2.** Plagioclase phenocryst with glassy inclusions in a mafic to intermediate volcanic rock fragment (Sample 190-1174B-1R-1, 6–10 cm [143.8 mbsf]) (plane-polarized light). **3.** Fine-grained sedimentary rock fragment (Sample 190-1174B-1R-1, 6–10 cm [143.8 mbsf]) (plane-polarized light). **4.** Slate fragment (Sample 190-1174B-9R-2, 108–112 cm [220.3 mbsf]) (cross-polarized light). **5.** Chert fragment with quartz veins (Sample 190-1174B-1R-1, 6–10 cm [143.8 mbsf]) (cross-polarized light). **6.** Silicic volcanic fragment with microphenocryts of quartz and feldspar (Sample 190-1174B-1R-1, 6–10 cm [143.8 mbsf]) (cross-polarized light).

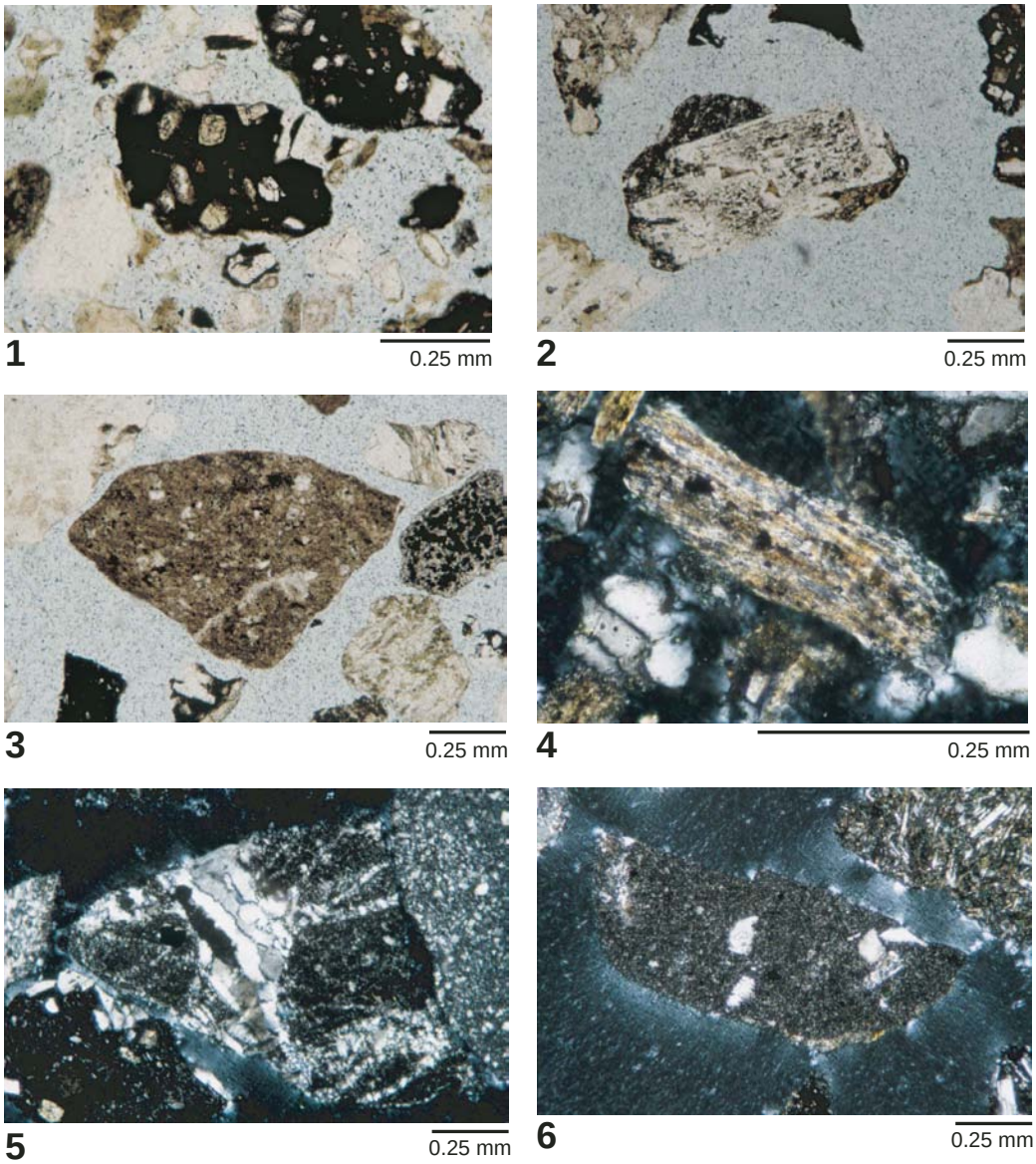

Plate P2. Photomicrographs illustrating mineral and lithic grains from sands at Sites 1175 and 1176, Leg 190, Nankai Trough trench wedge to slope transition. **1.** Quartzose sand with quartz, sedimentary rock fragments and chert (Sample 190-1176A-48X-CC, 14–17 cm [440.15 mbsf]) (cross-polarized light). **2.** Red radiolarian chert fragment with thin quartz veins (Sample 190-1176A-46X-CC, 19–23 cm [421 mbsf]) (plane-polarized light). **3.** Polygonal quartz grain with undulose extinction (Sample 190-1176A-46X-CC, 19–23 cm [421 mbsf]) (cross-polarized light). **4.** Radiolarian chert fragment containing quartz veins (Sample 190-1176A-46X-CC, 19–23 cm [421 mbsf]) (cross-polarized light). **5.** Metamorphic rock fragment with aligned quartz and muscovite (Sample 190-1176A-32X-CC, 7–9 cm [286.17 mbsf]) (cross-polarized light). **6.** Silicic tuffaceous fragment with relict shards in groundmass (Sample 190-1175A-37X-4, 30–32 cm [344.8 mbsf]) (plane-polarized light).

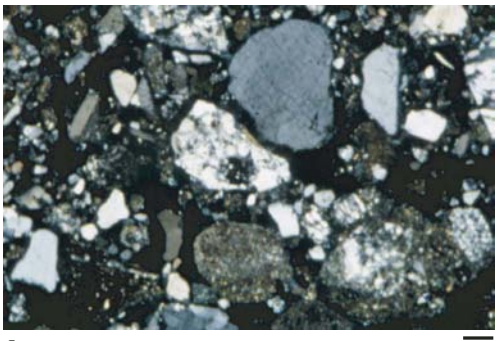

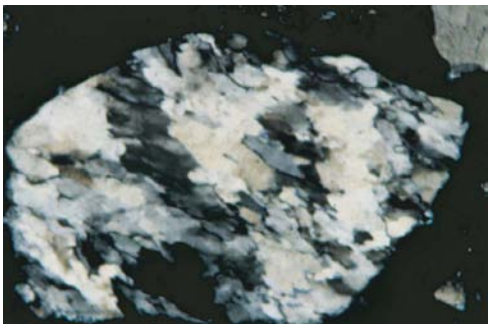

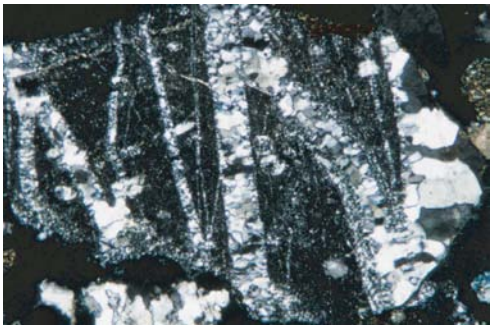

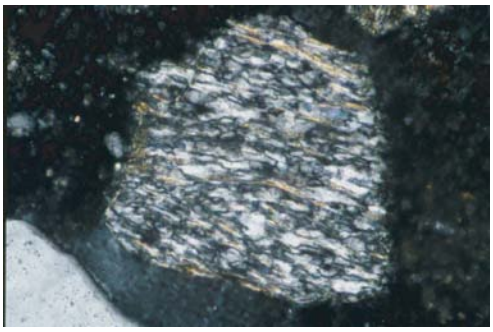

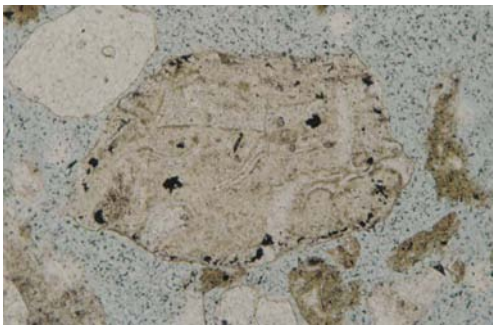

Plate P3. Photomicrographs illustrating mineral and lithic grains from sands/sandstones at Site 1177, Leg 190, Shikoku Basin turbidite facies Nankai Trough trench fill. **1.** Quartzose sandstone with quartz, plagioclase and quartzose sedimentary rock fragments (Sample 190-1177A-45R-1, 84–88 cm [723.74 mbsf]) (cross-polarized light). **2.** Devitrified silicic volcanic rock fragment (in center) amongst quartz and sedimentary rock fragments (Sample 190-1177A-45R-1, 84–88 cm [723.74 mbsf]) (cross-polarized light). **3.** Microcline with it diagnostic cross-hatched twinning (Sample 190-1177A-37R-3, 148–150 cm [648.88 mbsf]) (cross-polarized light). **4.** Very low grade metamorphic rock fragment with spaced dissolution cleavage (Sample 190-1177A-17R-1, 52–56 cm [454 mbsf]) (cross-polarized light). **5.** Banded rhyolite fragment (Sample 190-1177A-37R-3, 148–150 cm [648.88 mbsf]) (plane-polarized light). **6.** Silicic volcanic fragment with a rectangular biotite phenocryst (Sample 190-1177A-17R-1, 52–56 cm [454 mbsf]) (plane-polarized light).

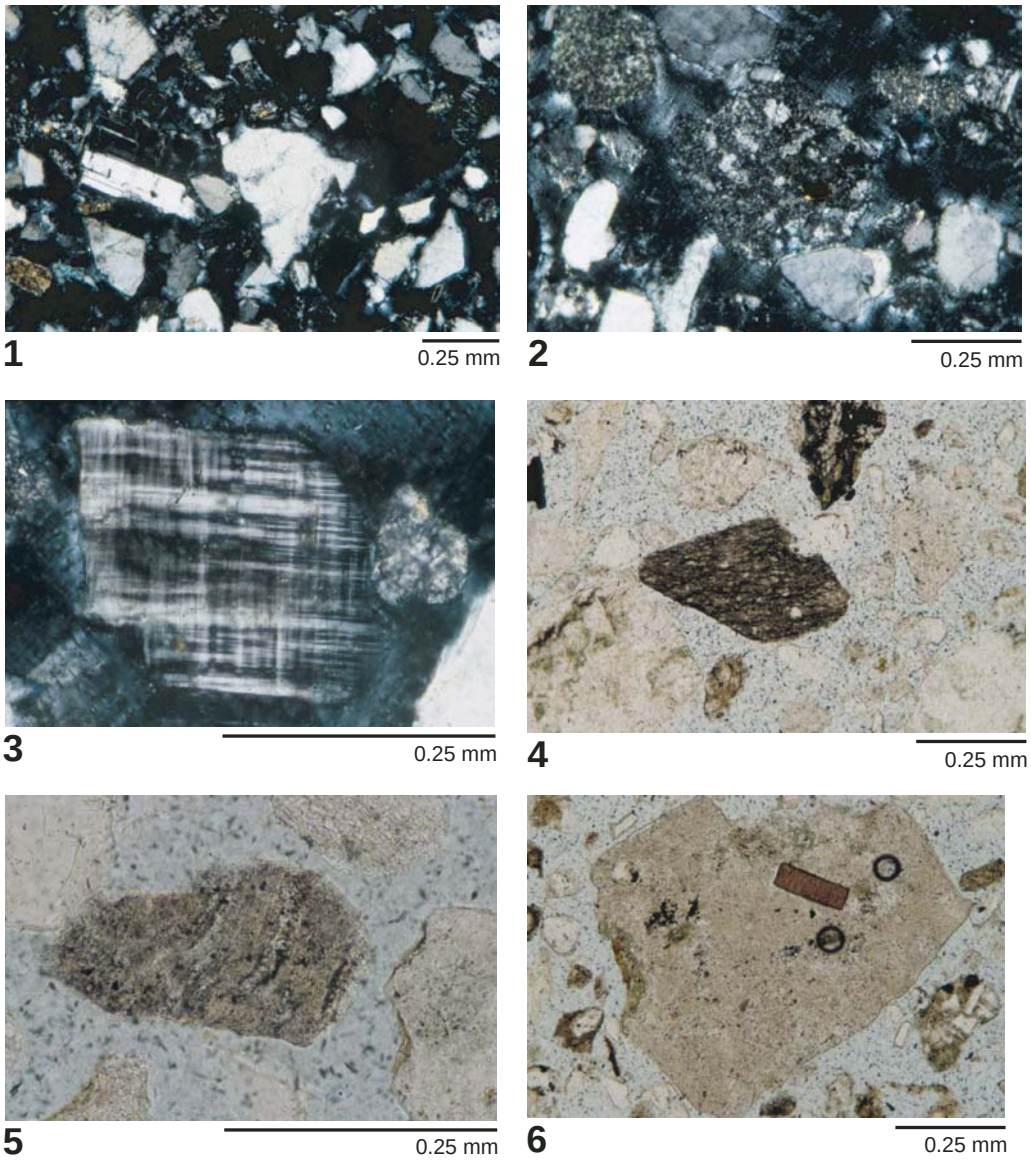

Plate P4. Photomicrographs illustrating mineral and lithic grains from sands/sandstones at Site 1178, Leg 190, Nankai Trough trench wedge (Sample 190-1178B-23R-2, 51–53 cm [613.7 mbsf]). **1.** Mudstone fragment with thin quartz vein (plane-polarized light). **2.** Mudstone fragment (plane-polarized light). **3.** Mudstone fragment (cross-polarized light). **4.** Radiolarian chert fragment with quartz veins (plane-polarized light). **5.** Mudstone fragment (plane-polarized light). **6.** Chert fragment with quartz veins (cross-polarized light).